

# Predicting electrical conductivity in bi-metal composites

Daniel N. Blaschke, John S. Carpenter, and Abigail Hunter

Oct. 1, 2024

Los Alamos National Laboratory, Los Alamos, NM, 87545, USA

E-mail: dblaschke@lanl.gov, carpenter@lanl.gov, ahunter@lanl.gov

## Abstract

Generating high magnetic fields requires materials with not only high electric conductivity, but also good strength properties in order to withstand the necessarily strong Lorentz forces. A number of bi-metal composites, most notably Cu/Nb, are considered to be good candidates for this purpose. Here, we generalize our previous work on Cu/Nb in order to predict, from theory, the dependence of electric conductivity on the microstructure and volume fraction of the less conductive component for a number of other bi-metal composites. Together with information on strength properties (taken from previous literature), the conductivity information we provide in this work can help to identify new promising candidate materials (such as Cu/Nb, Cu/Ag, Cu/W, ...) for magnet applications with the highest achievable field strengths.

## Contents

<b>1</b>	<b>Introduction</b>	<b>2</b>
<b>2</b>	<b>The model</b>	<b>3</b>
<b>3</b>	<b>Conductivity Results</b>	<b>4</b>
<b>4</b>	<b>Review of strength properties</b>	<b>6</b>
<b>5</b>	<b>Conclusion and Outlook</b>	<b>9</b>

# 1 Introduction

Studying fundamental questions and behaviors (such as phase transformations) in a wide range of materials systems such as semi- and super-conductors, quantum matter and thin films, often requires the creation of ultra-high magnetic fields ( $>80\text{T}$ ). The current world record for pulsed magnetic fields is  $100\text{ T}$ , which was set about a decade ago [1]. While there is high demand for use of such ultra-high magnetic field resources, access can still be limited for multiple reasons, one of them being the material properties of the conductive wire used within the magnet [2]. Currently, the  $100\text{ T}$  pulsed field magnet at the National High Magnetic Field Laboratory utilizes a Cu/Nb nano-composite wire for this purpose [2]. This wire is manufactured using an accumulative drawing and bonding (ADB) method that makes it difficult to produce consistent material properties from batch-to-batch and over the relatively long lengths required in the magnet [2]. Variation in material properties can cause experiments to either out-right fail, or have sub-par performance, resulting in costly delays and limitations in the availability of this resource.

These conductive wires are required to have a unique set of material properties. Particularly, in order to withstand the necessarily high Lorentz forces, the conductive winding wire utilized in these applications must have both high conductivity as well as exceptional strength properties [3–7]. For example, the current Cu/Nb wire has an ultimate tensile strength (UTS) of  $\sim 1\text{ GPa}$  and an electrical conductivity of  $\sim 70\%$  IACS (International Annealed Copper Standard) at room temperature [8, 9]. Furthermore, the wire needs to be fairly ductile as it is wound into coils to be used in the magnet [2]. Finally, these ultra-high pulsed field magnets operate at low temperatures ( $\sim 77\text{--}400\text{ K}$  [2]), so the material properties of the wires must be maintained through a range of temperatures. For example, at  $77\text{K}$ , Cu/Nb can exhibit very high electrical conductivities,  $\sim 300\%$  IACS and an UTS ranging from  $\sim 1\text{--}1.4\text{ GPa}$  [8, 9]. New composite materials with improved material properties regarding electrical conductivity and strength help to open the door for even higher pulsed magnetic fields, which would enable new experimental possibilities for several different classes of materials.

Promising material candidates for this purpose that so far have been identified include Cu/Nb [3, 8, 10, 11], Cu/stainless steel [10, 11], Cu/Cr [12], Cu/W [13, 14], Cu/Ta [15], and Cu/Ag [4, 16, 17]. All of these examples are two-phase composites which are fabricated using severe plastic deformation (SPD) methods such as ADB or accumulative roll bonding (ARB). Because it is currently used in ultra-high pulsed field magnets, the majority of previous literature has been focused on understanding and optimizing Cu/Nb. Thus, the material properties of Cu/Nb naturally become the baseline performance on which the community aims to improve upon. As mentioned, several other candidate materials have been investigated, and with the recent work in multi-principal element and high-entropy alloys, one can imagine a vast design space in which to explore.

The focus of this current work is on bi-metal composites, and as such we continue our previous study [18], of understanding and predicting electric conductivity based on the microstructure. Together with a separate study of material strength (not included here), this endeavor will help to identify new materials with even more optimized conductivity/strength properties for magnet applications. In particular, we generalize our previous theoretical study of Cu/Nb to a number of other bi-metals and identify the volume fraction the second (less conductive) component should not exceed in order to maintain good conductivity. A related recent numerical study of Cu/Nb composites can be found in Ref. [19].

The paper is organized as follows: We start in Section 2 by reviewing the modeling techniques, i.e. the phase field framework and the models predicting the contributions of the various microstructures to electric resistivity. We then proceed in Section 3 with presenting our simulation

results for electric conductivity of a number of bi-metals. Strength properties of those bi-metals are assembled from the literature, and we give an overview over promising candidates of strong and conductive bi-metals in Section 4.

## 2 The model

Like in our previous work [18] and following [20], we consider local charge density  $\rho_e$  as our order parameter within a phase field approach and (within our simulations) must apply an external electric field  $E_{\text{ex}}$ . The local electric field  $\mathbf{E}$  is generated by the spatial distribution of charge density  $\rho_e$  and the externally applied electric field, i.e.

$$\mathbf{E}(\mathbf{x}) = \mathbf{E}^{\text{ex}} - \frac{i}{\epsilon_0} \int \frac{d^3k}{(2\pi)^3} \frac{\tilde{\rho}_e(\mathbf{k})}{k^2} \mathbf{k} e^{i\mathbf{k}\mathbf{x}}, \quad (2.1)$$

where  $\tilde{\rho}_e$  is the Fourier transform of  $\rho_e$ . The local current density  $\mathbf{j}$  is then given (via the microscopic version of Ohm's law) by

$$j_i = \sigma_{ij} E_j(\mathbf{x}) = \sigma_{ij} E_j^{\text{ex}} - \frac{i\sigma_{ij}}{\epsilon_0} \int \frac{d^3k}{(2\pi)^3} \frac{k_j}{k^2} \tilde{\rho}_e(\mathbf{k}) e^{i\mathbf{k}\mathbf{x}}, \quad (2.2)$$

where conductivity  $\sigma$  may take a tensorial form to account for anisotropy. For simplicity, we however assume an isotropic approximation for  $\sigma_{ij} \approx \sigma \delta_{ij}$ .

The law of charge conservation,  $\dot{\rho}_e = -\nabla \cdot \mathbf{j}$ , is related to the Ginzburg-Landau equations within a phase-field formulation. Hence, evolving this equation will give us a final charge density distribution, which via Eqs. (2.1) and (2.2) yields a current distribution  $\mathbf{j}(\mathbf{x})$ , i.e.

$$\dot{\rho}_e = -\partial_i (\sigma E_i(\mathbf{x})) = -\partial_i (\sigma E_i^{\text{ex}}) - \frac{\sigma}{\epsilon_0} \int \frac{d^3k}{(2\pi)^3} \tilde{\rho}_e(\mathbf{k}) e^{i\mathbf{k}\mathbf{x}} + \frac{i}{\epsilon_0} (\partial_i \sigma) \int \frac{d^3k}{(2\pi)^3} \frac{k_i}{k^2} \tilde{\rho}_e(\mathbf{k}) e^{i\mathbf{k}\mathbf{x}}. \quad (2.3)$$

The experimentally measured macroscopic conductivity is then determined by spatially averaging  $\mathbf{j}$  and the macroscopic version of Ohm's law:

$$\langle j_i \rangle = \sigma^{\text{eff}} E_i^{\text{ex}}. \quad (2.4)$$

In order to model local conductivity  $\sigma$ , we assume Matthiessen's rule [21] holds, i.e. electric resistivity  $\rho = 1/\sigma$  is the sum of bulk resistivity  $\rho_0(T)$  and additional contributions to the bi-metal interfaces ( $\rho_i$ ), grain boundaries ( $\rho_{\text{gb}}$ ), and average dislocation density  $\rho_d$ . We neglect sub-leading contributions from vacancies, interstitial atoms, and other types of defects, assuming they are not prevalent in our samples. The three contributions to  $\rho$  can be modeled as follows [18, 22–25]:

The probability of scattering electrons at a bi-metal interface is parameterized by model parameter  $p \in [0, 1]$  and its value depends in the “roughness” of the bi-metal interface with typical values being in the vicinity of 0.5 [23]. The contribution to resistivity in the two phases of the bi-metal on either side of the interface stemming from such scattering events can be estimated as<sup>1</sup>

$$\rho_{\text{if}} = \rho_0(T) \left[ \frac{3}{8} (1-p) \lambda_0(T) \frac{1}{d_0} \right], \quad (2.5)$$

<sup>1</sup>Note that after careful consideration we realized the additional factor  $2V_f/(1-V_f)$  depending on the volume fraction  $V_f$  of the second phase (which is 1 for  $V_f = 1/3$ ) present in [18] should not be included. Also, we re-calibrated the fraction of layers  $\geq 100\text{nm}$  containing 2 grains (30% instead of 25%) as well as the standard deviation of the Gaussian distribution (50nm instead of 40nm); see the details given below in Sec. 3.

where  $d_0$  denotes the layer thickness, and  $\lambda_0$  is the electron mean free path. Both  $d_0$  and  $\lambda_0$  can be different on either side of the interface. Note that  $\rho_{\text{if}}$  increases significantly as the layer thickness shrinks to values competing the electron mean free path.

Likewise, grain boundary scattering becomes important when grain sizes are small so that they are comparable to  $\lambda_0$ . The according contribution to electric resistivity is estimated from the following expression:

$$\rho_{\text{gb}} = \rho_0(T) \left[ \left( 1 - \frac{3}{2}\alpha + 3\alpha^2 - 3\alpha^3 \ln(1 + 1/\alpha) \right)^{-1} - 1 \right],$$

$$\alpha = \frac{\lambda_0(T)}{d} \frac{R}{1-R}, \quad (2.6)$$

where the grain boundary reflection coefficient  $R \in [0, 1]$  depends on the size and shape of the single crystal grains. Grains in an ARB material with thin layers are typically long and flat [26], so that  $d$  (the grain “size”) is taken to mean the grain thickness perpendicular to the layer orientation.

Dislocation density, finally is parameterized by  $\rho_d = R_d N_d$ , where the “scattering power”  $R_d$  is typically of the order of  $10^{-25} \text{ } \Omega \text{m}^3$  [27] so that dislocation densities ( $N_d$ ) below  $10^{16} \text{m}^{-2}$  lead to negligible contributions to electric resistivity. Experiments with Cu/Nb have shown [18] that typical dislocation densities are below or close to  $10^{15} \text{m}^{-2}$ . Here, we assume this value for  $N_d$  in our simulations, even though its effect is in the sub-percent level and thus very small.

### 3 Conductivity Results

In our previous work, we showed that a typical Cu/Nb bi-metal exhibits a distribution in layer thickness, rather than equally thick layers, an effect that is even more pronounced when the volume fraction  $V_f$  differs from 0.5 [18, 28]. Furthermore, for sufficiently thin layers, most of those layers have only one single crystal grain across the layer thickness and a smaller fraction of layers of thicknesses beyond 100nm exhibit 2, and less frequently more grains across the thickness. Lacking details of the grain distribution, a rough first-order approximation, which led to good theoretical predictions for conductivity, was achieved by calibrating the fraction of layers thicker than 100nm to have 2 grains across the thickness [29], and only one grain otherwise. Combining this assumption with a Gaussian distribution in layer thickness led to good agreement with measured conductivity values for Cu/Nb with average layer thicknesses up to 150nm, as shown in our previous work [18]. Figure 1 illustrates these two steps: The blue curve within this figure shows the theory predictions when only one grain is present across each layer thickness (recalibrated in anticipation of Fig. 4 below). Adding two grains to 30% of thicker grains leads to a drop in conductivity in those thicker layers, as shown in orange. A Gaussian distribution over the layer thicknesses (calculated from the orange curve) yields the final prediction in green.

Assuming that the same ARB processing techniques leads to similar grain sizes, we now proceed to apply those same assumptions to predict conductivity for a number of other bi-metals of interest, in particular: Ag/Fe, Cu/Ag, Cu/Cr, Cu/Fe, Cu/Nb, Cu/Ta, and Cu/W. Note that more accurate predictions would require detailed knowledge of the grain distribution within each bi-metal, which would have to be measured. Lacking this knowledge, the next best thing we can do presently is to use the same calibration and assumptions which led to good agreement with our Cu/Nb experiments in Ref. [18].

In Figure 2 we show our simulation results for those bi-metals at room temperature and with average layer thicknesses of the first metal of 100nm as a function of volume fraction  $V_f$  of the second metal (which in most of our examples is the less conductive metal). The second metal’s

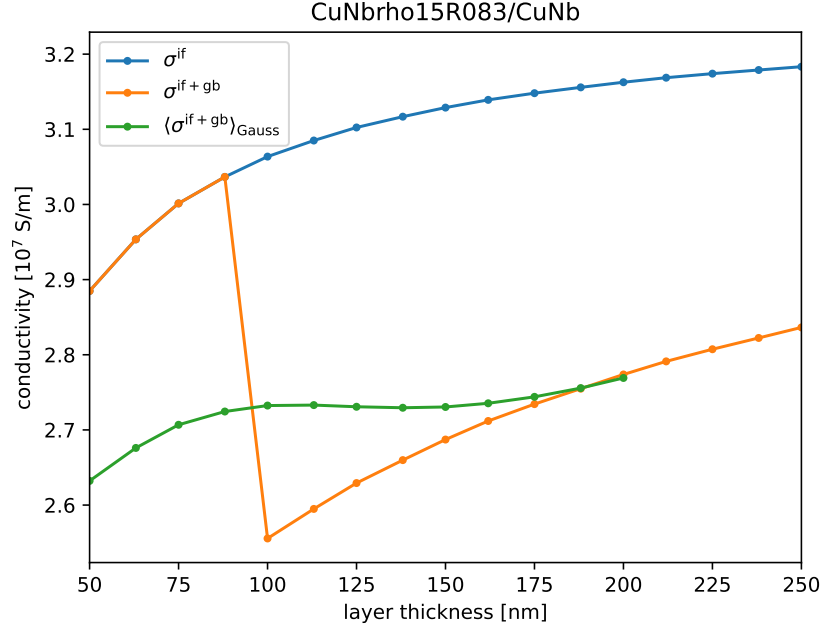


Figure 1: We show electric conductivity as a function of layer thickness for a Cu/Nb composite. The blue curve shows model results taking into account only the effect of interface scattering. For the orange curve, we have assumed 30% of the thicker layers ( $\geq 100$ nm) have 2 grains across the layer thickness. The green curve shows the effect of having a distribution of layer thicknesses and was computed using a Gaussian distribution of the results shown in orange with a standard deviation of 50nm. This rough calibration is based on our previous work, Ref. [18], using our own measured Cu/Nb data which exhibited a range of layer thicknesses within each sample.

layer thickness equals that of the first metal only at  $V_f = 0.5$  and is typically thinner when the second metal's volume fraction  $V_f < 0.5$  (see e.g. [22, 28]). Note that in cases where the second metal is significantly less conductive than the first, the volume fraction dependence is almost linear. The only exception here is Cu/Ag because both metals are good conductors in this case. Magnetic fields of about 100T are achievable with bi-metals with an electric conductivity of 60% IACS together with an ultimate tensile strength (UTS) of 1.2 GPa [7]. In order to push the highest achievable magnetic fields well beyond 100T (say up to 120T), the UTS needs to be even higher [30, 31], i.e. 1.5 GPa, without reducing electric conductivity below 55% IACS; this limit is indicated as a gray dashed line in Fig. 2. For most of the listed bi-metals, this means a volume fraction not much higher than 1/3 should be considered.

We therefore focus on  $V_f \approx 0.3$  for Figure 3 where we show the temperature dependence of electric conductivity for all bi-metals considered in this work. 55% IACS is again indicated in a dashed gray line, showing that this lower limit is exceeded even for the least conductive bi-metal, Cu/Fe, up to elevated temperatures of almost 350K. We see that the temperature dependence in the range we simulated, i.e. 100–450 K (in 50 K increments), is very similar across all simulated bi-metals.

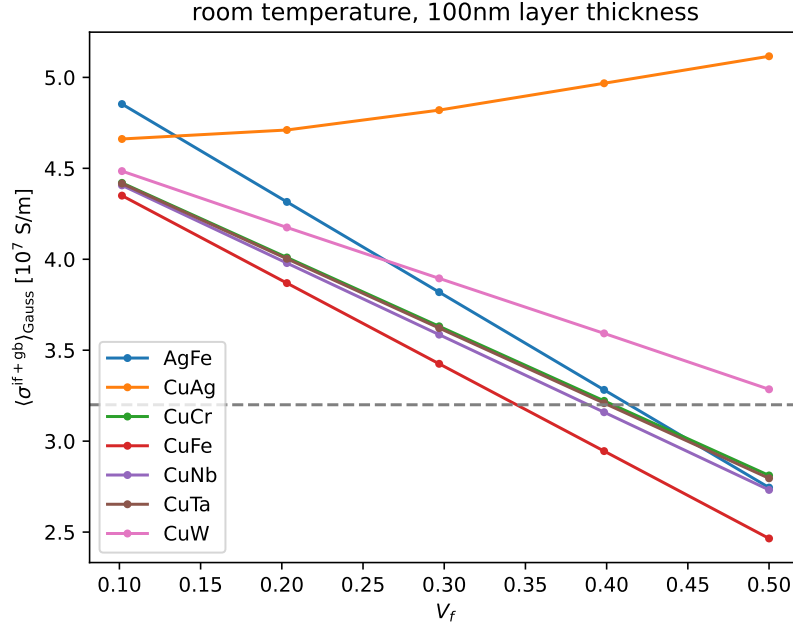


Figure 2: We show electric conductivity as a function of volume fraction for a number of bi-metal composites at room temperature. The average layer thickness of the first metal was 100nm, i.e. this was the mean value within a Gaussian distribution of layer thicknesses with 50nm standard deviation. The second metal’s layer thickness equals that of the first metal only at  $V_f = 0.5$  and is typically thinner when the second metal’s volume fraction  $V_f < 0.5$  (see e.g. [22, 28]); 30% of the thicker layers were assumed to have two single crystal grains across the thickness. The dashed gray line indicates the conductivity required in ultra-high magnetic field applications.

## 4 Review of strength properties

A number of bi-metals processed with various techniques have been studied with respect to their strength properties in the past. ADB Cu/Nb wires have been of particular interest with ultimate tensile strengths up to well beyond 1 GPa, see Refs. [10, 32, 34]. More recently, ARB as well as CARB (i.e. cross accumulative roll bonding, where every rolling step is undertaken perpendicular to the previous one) have been studied as well for a number of bi-metals including Cu/Nb, Cu/Ag, and Cu/Ta (among others). Strengths have been achieved up to 1.2 GPa [22], see also Refs. [15, 41]. Other processing techniques have been used as well, such as high pressure torsion (HPT) for e.g. Cu/Cr [12]. Apart from severe plastic deformation, researchers have also studied creating very strong bi-metals by reducing the grain sizes; for example the authors of Ref. [42] achieved strengths above 0.9 GPa with ultrafine grained Cu/W. Some of the studies mentioned above also measured electric conductivity of their bi-metal, such as e.g. Ref. [22] who achieved  $\sim 61\%$  IACS for ARB Cu/Nb, Ref. [12] who achieved 76 % IACS for HPT Cu/Cr, and Refs. [14, 28, 35]. Many others have focused solely on strength properties.

In Figure 4 we combine strength and conductivity data from the literature with our own conductivity simulation results where no conductivity was provided in the reference. Note that our simulations pertain to ARB materials, though we may expect those results to be close enough to the conductivity of ADB bi-metals, provided we simulated for layer thicknesses well above the

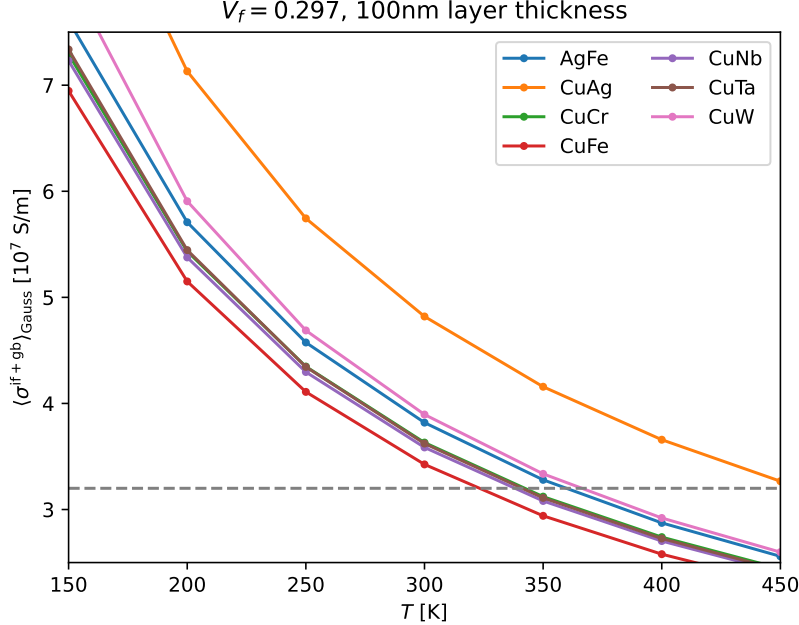


Figure 3: We show electric conductivity as a function of temperature for a number of bi-metal composites. The volume fraction of the second metal is  $V_f \approx 0.3$  in all of these simulations. The average layer thickness was 100nm, i.e. this was the mean value within a Gaussian distribution of layer thicknesses with 50nm standard deviation. 30% of the thicker layers were assumed to have two single crystal grains across the thickness. The dashed gray line indicates the conductivity required in ultra-high magnetic field applications.

electron mean free path for the (more conductive) matrix material. For those data where we have conductivity results from the literature, we compare to our own predictions and see that (as expected) they are very close if the bi-metal was processed with ARB, most notably the conductivity reported by Ding et al. [22]. As for ADB processed materials, as strength is increased through additional drawing and bonding steps, conductivity decreases, and therefore our ARB-optimized simulations overpredict conductivity for the ADB material (see Figure 4) since we do not account for the actual ADB microstructure in these cases. For this reason, the conductivity prediction for ADB Cu/Nb with UTS around 1.4 GPa shown in this figure is to be taken with a grain of salt: conductivity is likely somewhat lower than predicted.

For the purpose of Fig. 4, we assumed 100nm average layer thickness for the Cu phase in our simulations unless stated otherwise. Those results are meant to give readers an overview over bi-metals with promising strength and conductivity properties that are worth being studied further.

The main reason to study ARB instead of ADB is that ADB materials, do not necessarily have the desired shape and have been unreliable despite their initially good properties, i.e. fractured filaments are introduced during the preparation process [22, 35]. As we see from Figure 4, ARB materials have not achieved quite as high strength compared to ADB, but ARB has not been studied as long as ADB and researchers are constantly improving the former [22, 28, 43].

From Fig. 2, we see that a volume fraction of 1/3 or less for the less conductive material is necessary to achieve electric conductivities well above 55% IACS. Not surprisingly, many authors have thus focused on  $V_f = 1/3$ , as shown in Fig. 4. Clearly, ARB materials need to become even

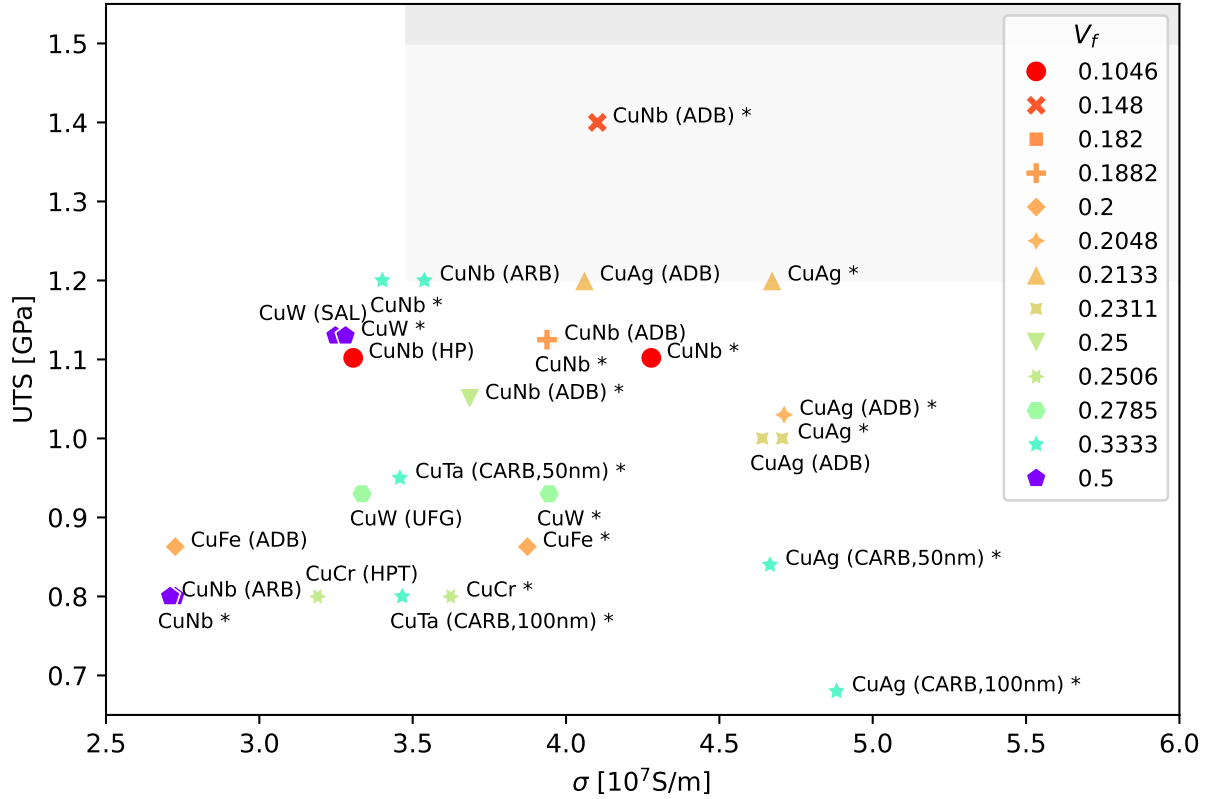


Figure 4: We show an overview over various bi-metal properties regarding strength and electric conductivity; the shaded area indicates the strength and conductivity requirements for generating magnetic fields of 100T and beyond. The material and processing method are indicated in the marker annotations, where ADB refers to ‘accumulative drawing and bonding’, ARB denotes ‘accumulative roll bonding’, CARB refers to ‘cross accumulative roll bonding’, UFG denotes ‘ultrafine grained’, HP refers to ‘hot pressed’, HPT is ‘high pressure torsion’, and ‘SAL’ is ‘self-assembled lamellar architecture’. The volume fraction of the second metal is indicated in the legend. For some roll bonded bi-metals, we also indicate the ‘nominal’ layer thickness, i.e. at a volume fraction of 1/3 the nominal layer thickness is that of the second metal and the Cu layer thickness is twice that number (or rather, two Cu layers are always bonded together). In all those cases where the electric conductivity was not reported, we use our own simulation result for the purpose of this plot, and indicate so by a star \*. Additionally, we compare our simulation results (for 100nm Cu layers within ARB) to all cases where conductivity was reported in the literature (indicated by a star \* once more). Experimental data are taken from Refs. [10, 22, 32–35] (Cu/Nb), [10, 36] (Cu/Fe), [15] (Cu/Ta) [37, 38] (Cu/Cr), [7, 16, 39–41] (Cu/Ag) [14, 42] (Cu/W).

stronger to meet the 1.5 GPa UTS requirement for the next generation magnets [30, 31]. In order to reach this goal, (one of) the currently most promising candidates, Cu/Ag, CuW, and Cu/Nb, would need to be made even stronger than the current highest results of 1.2 GPa reported by Ding et al. [22] for Cu/Nb.



## 5 Conclusion and Outlook

Ultrastrong magnetic fields require materials with high electric conductivity as well as high UTS to withstand the necessarily strong Lorentz forces. Pushing the limits beyond 100T has been a challenge and in order to aid with the identification of next generation materials for these applications, we calculated from theory electric conductivities for a number of bi-metals processed by ARB. Furthermore, we presented a survey of previous strength and conductivity results from the literature. The latter conductivities were subsequently compared to our predictions (see Fig. 4), which are fairly accurate for ARB, but (not surprisingly) often overpredict conductivity for ADB and otherwise processed bi-metals. Adapting our underlying model of microstructure together with accurate measurements of the actual microstructure will no doubt lead to more accurate predictions.

### Acknowledgments

This work was supported by the U.S. Department of Energy through Los Alamos National Laboratory, which is operated by Triad National Security, LLC, for the National Nuclear Security Administration of the U.S. Department of Energy under contract 89233218CNA000001. This work was funded through Los Alamos National Laboratory Directed Research and Development (LDRD) project ER20200375.

### References

- [1] T. Feder, “Magnetic record”, *Physics Today* **65** (2012) 30.
- [2] D. N. Nguyen, J. Michel, and C. H. Mielke, “Status and development of pulsed magnets at the NHMFL pulsed field facility”, *IEEE Trans. Appl. Supercond.* **26** (2016) 1–5.
- [3] S. Foner, “Experiments with strong pulsed magnetic fields produced by Cu/Nb microcomposite wire-wound magnets”, *Physica B* **155** (1989) 18–22.
- [4] L. Campbell, Y. Eyssa, P. Gilmore, P. Pernambuco-Wise, D. G. Parkin, D. G. Rickel, J. B. Schilligg, and H. J. Schneider-Muntau, “The US 100 T magnet project”, *Physica B* **211** (1995) 52–55.
- [5] J. D. Embury and K. Han, “Conductor materials for high field magnets”, *Curr. Opin. Solid State Mater. Sci.* **3** (1998) 304–308.
- [6] K. Han, J. Embury, J. Sims, L. Campbell, H.-J. Schneider-Muntau, V. Patsyrnyi, and A., “The fabrication, properties and microstructure of Cu-Ag and Cu-Nb composite conductors”, *Mater. Sci. Eng. A* **267** (1999) 99–114.
- [7] J. Freudenberger, W. Grünberger, E. Botcharova, A. Gaganov, and L. Schultz, “Mechanical properties of Cu-based micro- and macrocomposites”, *Adv. Eng. Mater.* **4** (2002) 677–681.
- [8] K. Han, V. Toplosky, R. Walsh, C. Swenson, B. Lesch, and V. Patsyrnyi, “Properties of high strength Cu-Nb conductor for pulsed magnet applications”, *IEEE Trans. Appl. Supercond.* **12** (2002) 1176–1180.
- [9] M. Liang, Y. Lu, Z. Chen, C. Li, G. Yan, C. Li, and P. Zhang, “Characteristics of high strength and high conductivity Cu-Nb micro-composites”, *IEEE Trans. Appl. Supercond.* **20** (2010) 1619–1621.
- [10] F. Dupouy, S. Askenazy, J. P. Peyrade, and D. Legat, “Composite conductors for high pulsed magnetic fields”, *Physica B* **211** (1995) 43–45.
- [11] V. Patsyrnyi, A. Shikov, A. Vorobieva, *et al.*, “High strength, high conductivity macro- and microcomposite winding wires for pulsed magnets”, *Physica B* **294-295** (2001) 669–673.
- [12] S. V. Dobatkin, J. Gubicza, D. V. Shangina, N. R. Bochvar, and N. Y. Tabachkova, “High strength and good electrical conductivity in Cu-Cr alloys processed by severe plastic deformation”, *Mater. Lett.* **153** (2015) 5–9.

- [13] L. Dong, G. Wei, T. Cheng, *et al.*, “Thermal conductivity, electrical resistivity, and microstructure of Cu/W multilayered nanofilms”, *ACS Appl. Mater. Interfaces* **12** (2020) 8886–8896.
- [14] T. Han, C. Hou, Z. Zhao, *et al.*, “Simultaneous enhancement of strength and conductivity via self-assembled lamellar architecture”, *Nature Commun.* **15** (2024) 1863.
- [15] L. F. Zeng, R. Gao, Q. F. Fang, X. P. Wang, Z. M. Xie, S. Miao, T. Hao, and T. Zhang, “High strength and thermal stability of bulk Cu/Ta nanolamellar multilayers fabricated by cross accumulative roll bonding”, *Acta Mater.* **110** (2016) 341–351.
- [16] Y. Sakai, K. Inoue, T. Asano, H. Wada, and H. Maeda, “Development of high-strength, high-conductivity Cu-Ag alloys for high-field pulsed magnet use”, *Appl. Phys. Lett.* **59** (1991) 2965–2967.
- [17] C. Zhao, Z. Xiaowei, E. Wang, R. Niu, and K. Han, “Simultaneously increasing strength and electrical conductivity in nanostructured Cu-Ag composite”, *Mater. Sci. Eng. A* **652** (2016) 296–304.
- [18] D. N. Blaschke, C. Miller, R. Mier, *et al.*, “Predicting electrical conductivity in Cu/Nb composites: a combined model-experiment study”, *J. Appl. Phys.* **132** (2022) 045105, arXiv:2204.03777 [cond-mat.mtrl-sci].
- [19] T. Shiraiwa, K. Yasuda, F. Briffod, *et al.*, “Materials informatics approach to Cu/Nb nanolaminate microstructure correlations with yield strength and electrical conductivity”, *Mater. Trans.* **65** (2024) 677–686.
- [20] Y. M. Jin, “Phase field modeling of current density distribution and effective electrical conductivity in complex microstructures”, *Appl. Phys. Lett.* **103** (2013) 021906.
- [21] A. Matthiessen and C. Vogt, “IV. On the influence of temperature on the electric conducting-power of alloys”, *Philos. Trans. R. Soc. Lond.* **154** (1864) 167–200.
- [22] C. Ding, J. Xu, D. Shan, B. Guo, and T. G. Langdon, “Sustainable fabrication of Cu/Nb composites with continuous laminated structure to achieve ultrahigh strength and excellent electrical conductivity”, *Compos. B Eng.* **211** (2021) 108662.
- [23] L. Tian, I. Anderson, T. Riedemann, and A. Russell, “Modeling the electrical resistivity of deformation processed metal-metal composites”, *Acta Mater.* **77** (2014) 151–161.
- [24] R. B. Dingle and W. L. Bragg, “The electrical conductivity of thin wires”, *Proc. Royal Soc. Lond.* **A201** (1950) 545–560.
- [25] K. Fuchs, “The conductivity of thin metallic films according to the electron theory of metals”, *Math. Proc. Camb. Philos. Soc.* **34** (1938) 100–108.
- [26] Y. Zhang, J. G. Gigax, T. J. Nizolek, J. S. Carpenter, M. M. Schneider, N. Li, L. Capolungo, and R. J. McCabe, “Tensile and failure behaviors of Cu/Nb nanolaminates: the effects of loading direction, layer thickness, and annealing”, *Acta Mater.* **240** (2022) 118346.
- [27] R. A. Brown, “Electrical resistivity of dislocations in metals”, *J. Phys. F: Met. Phys.* **7** (1977) 1283–1295.
- [28] J. S. Carpenter, C. Miller, D. N. Blaschke, W. P. Winter, and S. M. Thomas, “Optimizing conductivity and hardness in Cu–Nb nanolamellar composites fabricated through accumulative roll bonding without intermittent heat treatments”, *Metall. Mater. Trans. A* **54** (2023) 3691–3696.
- [29] J. S. Carpenter, R. J. McCabe, I. J. Beyerlein, T. A. Wynn, and N. A. Mara, “A wedge-mounting technique for nanoscale electron backscatter diffraction”, *J. Appl. Phys.* **113** (2013) 094304.
- [30] J.-B. Dubois, L. Thilly, P.-O. Renault, and F. Lecouturier, “Cu-Nb nanocomposite wires processed by severe plastic deformation: Effects of the multi-scale microstructure and internal stresses on elastic-plastic properties”, *Adv. Eng. Mater.* **14** (2012) 998–1003.
- [31] N. R. Council, *High Magnetic Field Science and Its Application in the United States: Current Status and Future Directions*, (Washington, DC: The National Academies Press, 2013).
- [32] J. Bevk, J. P. Harbison, and J. L. Bell, “Anomalous increase in strength of in situ formed Cu-Nb multifilamentary composites”, *J. Appl. Phys.* **49** (1978) 6031–6038.
- [33] R. Lei, S. Xu, M. Wang, and H. Wang, “Microstructure and properties of nanocrystalline copper-niobium alloy with high strength and high conductivity”, *Mater. Sci. Eng. A* **586** (2013) 367–373.

- [34] A. B. Rozhnov, V. I. Patsyrny, A. Kraynev, S. Rogachev, S. Nikulin, N. Khlebova, M. Polikarpova, and M. Zadorozhnyy, “Low-cycle bending fatigue and electrical conductivity of high-strength Cu/Nb nanocomposite wires”, *Int. J. Fatigue* **128** (2019) 105188.
- [35] J. S. Carpenter, C. Miller, D. J. Savage, D. R. Coughlin, E. L. Tegtmeier, and W. P. Winter, “The impact of rolling at temperature on conductivity and texture in nanolamellar Cu/Nb bimetallic composites”, *Metall. Mater. Trans. A* **53** (2022) 2208–2213.
- [36] F. Yang, L. Dong, L. Zhou, N. Zhang, X. Zhou, X. Zhang, and F. Fang, “Excellent strength and electrical conductivity achieved by optimizing the dual-phase structure in Cu-Fe wires”, *Mater. Sci. Eng. A* **849** (2022) 143484.
- [37] Q. Mao, L. Wang, J. Nie, and Y. Zhao, “Enhancing strength and electrical conductivity of Cu-Cr composite wire by two-stage rotary swaging and aging treatments”, *Compos. B Eng.* **231** (2022) 109567.
- [38] A. S. Prosviryakov and A. I. Bazlov, “Characterization of nanostructured CuCr bulk composites prepared by high-energy mechanical alloying”, *Mater. Chem. Phys.* **177** (2016) 1–7.
- [39] S. I. Hong and M. A. Hill, “Mechanical stability and electrical conductivity of Cu-Ag filamentary microcomposites”, *Mater. Sci. Eng. A* **264** (1999) 151–158.
- [40] W. Grünberger, M. Heilmaier, and L. Schultz, “Microstructure and mechanical properties of Cu-Ag microcomposites for conductor wires in pulsed high-field magnets”, *Int. J. Mater. Res.* **93** (2002) 58–65.
- [41] C. You, W. Xie, S. Miao, T. Liang, L. Zeng, X. Zhang, and H. Wang, “High strength, high electrical conductivity and thermally stable bulk Cu/Ag nanolayered composites prepared by cross accumulative roll bonding”, *Mater. Des.* **200** (2021) 109455.
- [42] T. Han, C. Hou, Z. Zhao, X. Huang, F. Tang, Y. Li, and X. Song, “W-Cu composites with excellent comprehensive properties”, *Compos. B Eng.* **233** (2022) 109664.
- [43] S. M. Ghalehbandi, M. Malaki, and M. Gupta, “Accumulative roll bonding—A review”, *Appl. Sci.* **9** (2019) 3627.